Supporting Information:

Probing hydrogen bonding orbitals: resonant inelastic soft x-ray scattering of aqueous NH_3

L. Weinhardt[1,2,3,4*], E. Ertan[5], M. Iannuzzi[6], M. Weigand[7], O. Fuchs[7], M. Bär[8,9], M. Blum[2,10], J.D. Denlinger[10], W. Yang[10], E. Umbach[1,7], M. Odelius[5], and C. Heske[1,2,3,4]

[1]*Institute for Photon Science and Synchrotron Radiation, Karlsruhe Institute of Technology (KIT), Hermann-v.-Helmholtz-Platz 1, 76344 Eggenstein-Leopoldshafen, Germany*

[2]*Department of Chemistry and Biochemistry, University of Nevada, Las Vegas (UNLV), NV 89154-4003, USA*

[3]*Institute for Chemical Technology and Polymer Chemistry, Karlsruhe Institute of Technology (KIT), Engesserstr. 18/20, 76128 Karlsruhe, Germany*

[4]*ANKA Synchrotron Radiation Facility, Karlsruhe Institute of Technology (KIT), Hermann-v.-Helmholtz-Platz 1, 76344 Eggenstein-Leopoldshafen, Germany*

[5]*Department of Physics, Stockholm University, AlbaNova University Centre, 10691 Stockholm, Sweden*

[6]*Institute of Chemistry, University of Zurich, Winterthurerstr. 190, CH-8057 Zurich, Switzerland*

[7]*Universität Würzburg, Experimentelle Physik VII, Am Hubland, 97074 Würzburg, Germany*

[8]*Helmholtz-Zentrum Berlin für Materialien und Energie GmbH, Renewable Energy, Hahn-Meitner-Platz 1, 14109 Berlin, Germany*

[9]*Institut für Physik und Chemie, Brandenburgische Technische Universität Cottbus-Senftenberg, Platz der Deutschen Einheit 1, 03046 Cottbus, Germany*

[10]*Advanced Light Source, Lawrence Berkeley National Laboratory, 1 Cyclotron Road, Berkeley, CA 94720, USA*

*corresponding author: lothar.weinhardt@kit.edu

Calculated x-ray absorption and emission spectra

Complementary to the spectrum sampling in CP2K (Fig. 1 of the main paper) and the molecular dynamics simulations of NH_3 in aqueous solution (Fig. 6 of the main paper), we also simulated x-ray absorption (XAS) and x-ray emission (XES) spectra for a series of $NH_3(H_2O)_n$ = 0, 4, 5, and 6 clusters in distinct hydrogen bonding configurations, as presented in Figure S1. The clusters were optimized within density functional theory in Gaussian 09[1] using the B3LYP functional[2] and the aug-cc-pVTZ basis set[3].

Subsequent spectrum calculations were performed in StoBe[4] using the Becke Perdew gradient-corrected exchange and correlation functionals[5–7]. For the core-excited nitrogen atom, a flexible IGLO basis set[8] was used. The oxygen atoms were described using effective core potentials (ECPs)[9], in conjunction with a 311/211 basis set for the valence electrons. The hydrogen atoms were described by a double-zeta basis set[10]. The auxiliary basis sets for nitrogen and oxygen were comprised of five s and two spd functions to fit both, the Coulomb and exchange correlation potentials. For hydrogen, the GENA4 procedure in StoBe was used to generate an auxiliary basis set.

The x-ray emission spectra were simulated based on the ground state Kohn-Sham eigenstates, whereas for the x-ray absorption spectra the half core-hole transition potential method[11] was used in combination with a double-basis set procedure in which, after convergence, the basis set was

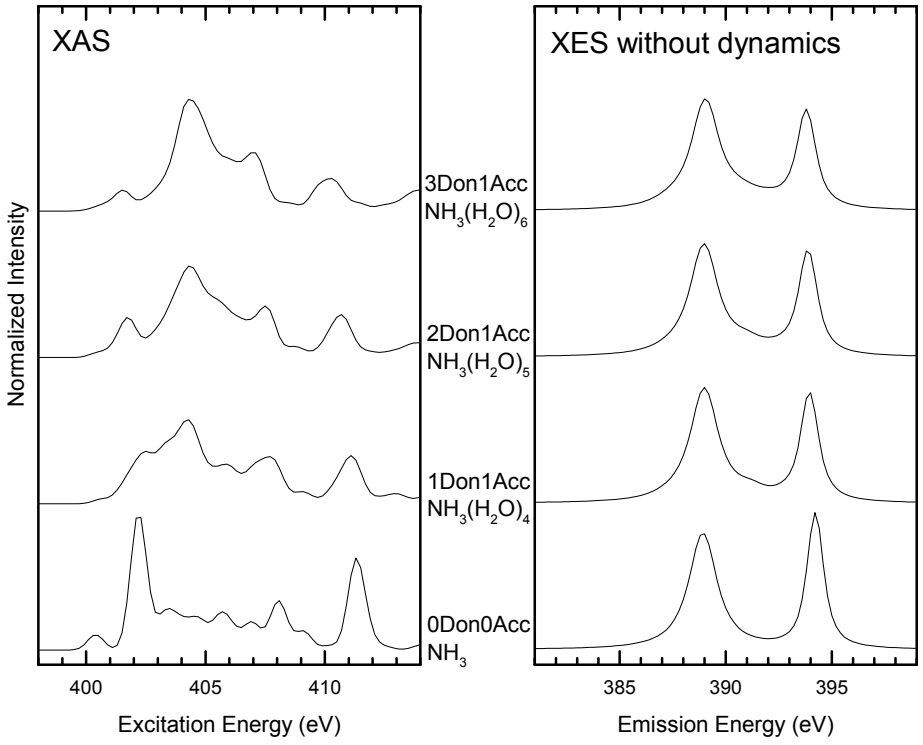

FIG. S1. Simulated N K XAS and XES spectra (without core-hole dynamics) for NH_3 in different H-bond environments, obtained from optimization of $NH_3(H_2O)_{n=0,4,5,6}$ clusters. The simulations were performed in StoBe, using the electronic ground state for XES and the half-core-hole transition potential method for XAS. The configurations for isolated NH_3 and for NH_3 with one accepting and two donating H-bonds are the same as used in Fig. 6. Donor-acceptor configurations are denoted as, e.g., 3Don1Acc for a three-donor, one-acceptor configuration.

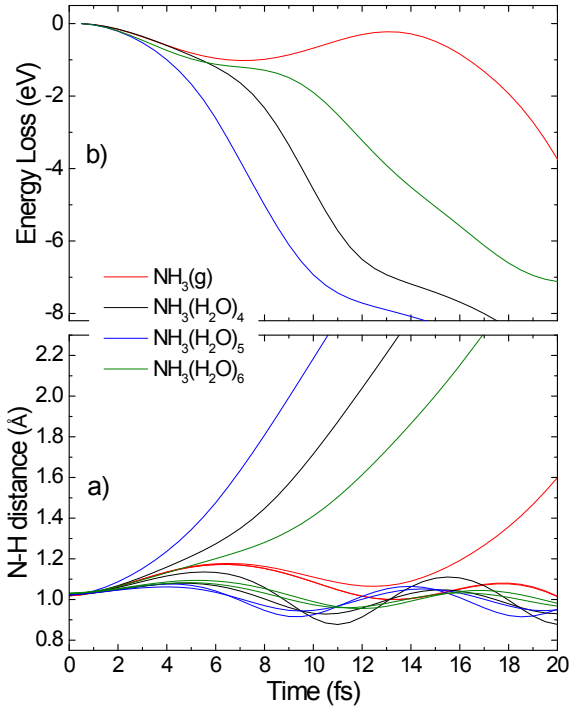

FIG. S2 a) Nuclear response in the lowest core-excited state, as simulated using StoBe. The configurations for isolated NH_3 and for NH_3 with one accepting and two donating H-bonds are the same as used in Fig. 6. b) Evolution of the energy loss at the Rayleigh line for excitation in the lowest core-excited state. The simulations were performed in StoBe. The configurations for isolated NH_3 and for NH_3 with one accepting and two donating H-bonds are the same as used in Fig. 6.

augmented with a large, diffuse basis set[12]. The calculated spectra were shifted in energy for approximate alignment to the experimental data.

To include dynamical effects in the x-ray emission spectra, we sampled the configurations from dynamics in the core-excited state and core-ionized state, respectively. Trajectories of 20 fs were obtained from Born-Oppenheimer ab initio molecular dynamics with a time-step of 0.5 fs. The geometric changes in the core-ionized state (not shown) are small, whereas the ammonia molecule undergoes N-H dissociation in the lowest N1s core-excited state. As seen in Figure S2a, the dissociation is ultra-fast and exhibits a solvation dependence. There is a considerable energy release during the N-H dissociation (Figure S2b), which gives rise to the inelastic tail (labeled V) in the "elastic" peak in Figure 5 of the main paper. The differences in geometric response between core-ionization and core-excitation for both, the isolated and solvated ammonia molecule, are responsible for the spectral differences displayed in Figure 6 in the main paper.

Calculated Spectator Shifts

To analyze trends and deviations between different computational setups (and compare with experiments), Table S1 presents the full set of calculated N K-edge absorption (top) and valence transition (center) energies of NH_3(g). Furthermore, the resulting emission energies (i.e., the difference between core absorption and valence transition energy) are also shown (bottom). The latter correspond to the values shown in Table 1 of the main paper for two of the different computational setups (A and E, see discussion below).

The results are obtained with scalar relativistic effects and spin-orbit coupling CASPT2 calculations [13] within the Douglas-Kroll-Hess formulation [14,15], using the state-interaction scheme in MOLCAS 8.0[16]. As in the main paper, we use the ANO-RCC-VTZP basis set and ten electrons distributed in 13 active orbitals. The core 1s orbital was placed in RAS3 and the remaining 12 orbitals were in placed in RAS2. The ground state and valence-excited state orbitals are generated from optimized ground state orbitals and the core excited state orbitals from optimization of the

Table S1: Calculated x-ray emission, x-ray absorption, and transition energies of NH_3(g) using different computational setups. Experimental absorption energies from Ref. [13]. Calculations have an accuracy of ±0.02 eV.

	(A) 21/20 R E(eV)	(B) 21/3(20) R E(eV)	(C) 21/3 R E(eV)	(D) 21/3 E(eV)	(E) NoSA R E(eV)	Exp E(eV)
Absorption energies						
$1s^{-1}4a_1^1$	401.29	401.04	400.77	400.89	401.07	400.71
$1s^{-1}2e^1$	402.93	402.68	402.40	402.54	402.57	402.33
$1s^{-1}5a_1^1$	403.50	-	-	-	-	402.91
Transition energies						
$3a_1 \rightarrow 4a_1$	6.45	6.32	6.31	6.56	6.83	
$3a_1 \rightarrow 2e$	8.24	8.12	8.09	8.18	8.18	
$3a_1 \rightarrow 5a_1$	8.64	8.54	-	-	-	
$1e \rightarrow 4a_1$	12.06	11.84	11.80	12.03	-	
$1e \rightarrow 2e$	13.87	13.62	13.59	12.06	-	
$1e \rightarrow 5a_1$	14.30	-	-	-	-	
X-ray emission energies						
$3a_1^{-1}4a_1^1$	394.84	394.72	394.47	394.34	394.24	394.1
$3a_1^{-1}2e^1$	394.69	394.57	394.31	394.36	394.39	394.5
$3a_1^{-1}5a_1^1$	394.87	-	-	-	-	394.6
$1e_1^{-1}4a_1^1$	389.23	389.21	388.97	388.84	-	388.6
$1e_1^{-1}2e^1$	389.06	389.06	388.81	388.82	-	388.5
$1e_1^{-1}5a_1^1$	389.20	-	-	-	-	388.6

core ionized orbitals. The 1s orbital is then frozen throughout the subsequent RASPT2 calculations.

To gain an understanding of how the basis set and the number of states included in the state-averaging affect the calculated emission energies, we performed a series of calculation where the computational setup was altered by variation in the number of excitations (valence and/or core) used for the state averaging as well as the determination of the spin-orbit coupling and the oscillator strengths. Furthermore, in some cases, we added a basis set consisting of one s, one p, and one d diffuse function to account for the Rydberg states.

In setup (A), we included 21 valence excitations and 20 core excitations and accounted for the Rydberg states (labeled "21/20 R" in Tab. S1). In contrast, setup (B), while 20 core-excitations were included in the state-averaging calculation, only a part of these were used in the spin-orbit coupling and the oscillator strengths calculations (3 instead of 20 – labeled "21/3(20) R" in Tab. S1). In setup (C), we also reduced the number of core excitations in the state-averaging calculations (i.e., from 20 to 3 – "21/3 R" in Tab. S1). Setup (D) was the same as setup (C), but without account for the Rydberg states in the basis set ("21/3"). In setup (E), we calculated the transitions without state-averaging, but did account for the Rydberg states in the basis set ("NoSA R"). Due to convergence issues, we did not manage to calculate values for excitation into the $5a_1$ absorption resonance for this computational setup. For setups (B), (C), and (D), no values for $5a_1$ excitation could be calculated since only 3 core excited states were included in the state interaction calculation.

The comparison of experimental and calculated emission energy shifts as a function of absorption resonance (i.e., spectator shifts) in connection with Table 1 of the main paper shows a good agreement when state-specific calculations (i.e., without state-averaging) are performed. In contrast, the state-averaged values show a small shift in the opposite direction. Close inspection of the values in Table S1 shows that the difference between the $4a_1$ and 2e absorption energies is largely independent of the different calculation setups used. In contrast, all state-averaged $3a_1 \rightarrow 4a_1$ transition energies are significantly lowered as compared to the state-specific values and thus predict a spectator shift of opposite sign compared to the experiment (note that the effect is amplified by taking the Rydberg states into account). In contrast, the $3a_1 \rightarrow 2e$ transition energies are very similar between state-averaged and state-specific calculations.

References:

1 M. J. Frisch, G. W. Trucks, H. B. Schlegel, G. E. Scuseria, M. A. Robb, J. R. Cheeseman, G. Scalmani, V. Barone, B. Mennucci, G. A. Petersson, H. Nakatsuji, M. Caricato, X. Li, H. P. Hratchian, A. F. Izmaylov, J. Bloino, G. Zheng, J. L. Sonnenberg, M. Hada, M. Ehara, K. Toyota, R. Fukuda, J. Hasegawa, M. Ishida, T. Nakajima, Y. Honda, O. Kitao, H. Nakai, T. Vreven, J. A. Montgomery Jr., J. E. Peralta, F. Ogliaro, M. J. Bearpark, J. Heyd, E. N. Brothers, K. N. Kudin, V. N. Staroverov, R. Kobayashi, J. Normand, K. Raghavachari, A. P. Rendell, J. C. Burant, S. S. Iyengar, J. Tomasi, M. Cossi, N. Rega, N. J. Millam, M. Klene, J. E. Knox, J. B. Cross, V. Bakken, C. Adamo, J. Jaramillo, R. Gomperts, R. E. Stratmann, O. Yazyev, A. J. Austin, R. Cammi, C. Pomelli, J. W. Ochterski, R. L. Martin, K. Morokuma, V. G. Zakrzewski, G. A. Voth, P. Salvador, J. J. Dannenberg, S. Dapprich, A. D. Daniels, Ö. Farkas, J. B. Foresman, J. V. Ortiz, J. Cioslowski and D. J. Fox, *Gaussian 09*, Gaussian, Inc., Wallingford, CT, USA, 2009.

2 A. D. Becke, *The Journal of Chemical Physics*, 1993, **98**, 5648–5652.

3 R. A. Kendall, T. H. D. Jr and R. J. Harrison, *The Journal of Chemical Physics*, 1992, **96**, 6796–6806.

4 *StoBe-deMon version 3.3 (2014), K. Hermann and L.G.M. Pettersson, M.E. Casida, C. Daul, A. Goursot, A. Koester, E. Proynov, A. St-Amant, and D.R. Salahub. Contributing authors: V. Carravetta, H. Duarte, C. Friedrich, N. Godbout, M. Gruber, J. Guan, C. Jamorski, M. Leboeuf, M. Leetmaa, M. Nyberg, S. Patchkovskii, L. Pedocchi, F. Sim, L. Triguero, and A. Vela.*, .

5 A. D. Becke, *Phys. Rev. A*, 1988, **38**, 3098–3100.

6 J. P. Perdew, *Phys. Rev. B*, 1986, **33**, 8822–8824.

7 J. P. Perdew, *Phys. Rev. B*, 1986, **34**, 7406–7406.

8 W. Kutzelnigg, U. Fleischer and M. Schindler, *NMR Basic Principles and Progress*, Springer, Heidelberg, 1990.

9 L. G. M. Pettersson, U. Wahlgren and O. Gropen, *The Journal of Chemical Physics*, 1987, **86**, 2176–2184.

10 N. Godbout, D. R. Salahub, J. Andzelm and E. Wimmer, *Can. J. Chem.*, 1992, **70**, 560–571.

11 L. Triguero, L. G. M. Pettersson and H. Ågren, *Phys. Rev. B*, 1998, **58**, 8097–8110.

12 H. Ågren, V. Carravetta, O. Vahtras and L. G. M. Pettersson, *Theor Chem Acta*, 1997, **97**, 14–40.

13 K. Andersson, P.-Å. Malmqvist and B. O. Roos, *The Journal of Chemical Physics*, 1992, **96**, 1218–1226.

14 M. Douglas and N. M. Kroll, *Annals of Physics*, 1974, **82**, 89–155.

15 B. A. Hess, *Phys. Rev. A*, 1986, **33**, 3742–3748.
16 F. Aquilante, L. De Vico, N. Ferré, G. Ghigo, P.-Å. Malmqvist, P. Neogrády, T. B. Pedersen, M. Pitoňák, M. Reiher, B. O. Roos, L. Serrano-Andrés, M. Urban, V. Veryazov and R. Lindh, *J. Comput. Chem.*, 2010, **31**, 224–247.